Available online at www.sciencedirect.com
SCIENCE DIRECT®
Journal of Magnetic Resonance 160 (2003) 97–106
JMR Journal of Magnetic Resonance
www.elsevier.com/locate/jmr

X-filtering for a range of coupling constants: application to the detection of intermolecular NOEs

Klaus Zangger,[a,*] Monika Oberer,[b] Walter Keller,[b] and Heinz Sterk[a]

[a] *Institute of Chemistry/Organic and Bioorganic Chemistry, University of Graz, Heinrichstrasse 28, A-8010 Graz, Austria*
[b] *Institute of Chemistry/Physical Chemistry, University of Graz, Heinrichstrasse 28, A-8010 Graz, Austria*

Received 15 May 2002; revised 23 August 2002

Abstract

A new method for heteronuclear X-filtering is presented, which relies on repetitive applications of $90°(^1H)$–$\tau(1/4^1J_{HC})$–$180°(^1H,^{13}C)$–$\tau(1/4^1J_{HC})$–$90°(^1H,^{13}C)$–PFG building blocks employing gradient-mediated suppression of magnetization built up for directly heteronuclear coupled protons. Thereby, a range of heteronuclear coupling constants can be suppressed by varying the delays of scalar coupling evolution both within and between individual transients. To achieve efficient destruction of ^{13}C-coupled protons in macromolecular systems, the scalar coupling evolution delays were optimized using simulated annealing by including transverse relaxation effects. With a combination of regular hard pulses, delays and pulsed field gradients only, this method yields sufficient X-filtering to allow the observation of intermolecular nuclear overhauser effects in a molecular complex consisting of a ^{13}C, ^{15}N double-labeled, and an unlabeled protein. This is achieved by exciting magnetization of ^{12}C- and ^{14}N-bound protons and detecting ^{13}C-bound ^1H magnetization in a 3D ^{13}C-filtered, ^{13}C-edited NOESY–HSQC experiment. The method is tested on the 18 kDa homodimeric bacterial antidote ParD.

Keywords: Homodimeric proteins; Intermolecular NOEs; NOESY–HSQC; ParD; X-filter

1. Introduction

The determination of 3D structures of proteins in solution by NMR spectroscopy has advanced quite rapidly within the past decades with high resolution structures now available up to ~35 kDa [1–3]. Through-space nuclear overhauser effects (NOEs) constitute by far the most important constraints for such NMR structure determinations [4]. Many proteins dimerize in solution or form even higher aggregates and this leads to ambiguities in the assignment of NOEs. Either some prior knowledge of the 3D structure, from e.g., a crystal structure [5], a homologous protein [6], or experimental techniques are necessary to separate intermolecular from intramolecular NOEs. Maybe the most intuitive experimental method for the determination of intermolecular NOEs is based on using mixtures of deuterated and protonated molecules [7,8]. For homodimeric proteins a 1:1 mixture of deuterated and protonated samples allows the identification of intermolecular NOEs through the reduction in intensity of intermonomer NOEs versus intramonomer NOEs when compared to a NOESY experiment on fully protonated samples. However, this approach may not be feasible for a particular protein due to limited or unsuccessful expression of a fully deuterated sample. In addition the high cost of a fully deuterated protein also limits its use. To date the most efficient experimental method for the distinction of intermolecular NOEs in homodimeric proteins has been selective ^{13}C and ^{15}N labeling of one monomer. Thereby, a sample of unlabeled protein is mixed with an equimolar solution of labeled protein, resulting in a solution containing 50% labeled–unlabeled dimer together with 25% labeled–labeled and 25% unlabeled–unlabeled dimers. Intermolecular NOEs can then be separated in the 50% labeled–unlabeled dimer when ^1H magnetization is monitored that either starts at ^{12}C- or ^{14}N-bound protons, is transferred via isotropic mixing,

* Corresponding author. Fax: +43-316-380-9840.
E-mail address: klaus.zangger@kfunigraz.ac.at (K. Zangger).

1090-7807/03/$ - see front matter © 2003 Elsevier Science (USA). All rights reserved.
doi:10.1016/S1090-7807(02)00176-3

and subsequently detected at ^{13}C-bound protons, or vice versa [9–17]. Therefore, a period, where protons bound to ^{13}C are selected for (editing), as well as one, where the magnetization of protons bound to ^{13}C and ^{15}N is suppressed (filtering), have to be combined in one pulse-sequence separated by an isotropic mixing period. Selecting protons bound to ^{13}C can be achieved very effectively using routine gradient-enhanced NMR techniques [18]. On the other hand selecting only protons bound to carbon-12 (^{13}C-filtering) in the presence of ^{13}C-bound protons constitutes a major problem due to the relatively wide range of possible ^{1}H–^{13}C one bond scalar coupling constants [9,19–23]. The most often used building block for X-filtering, $90°(^{1}H)$–$1/4^{1}J_{HX}$–$180°(^{1}H,X)$–$1/4^{1}J_{HX}$–$90°(X)$, destroys the magnetization of X-bound protons through the conversion of antiphase proton magnetization to undetectable double- and zero quantum magnetization by the last 90° X pulse if the delays are tuned to $1/4^{1}J_{HX}$ [21,22]. However, the typical range of proton–carbon coupling constants (usually 120–160 Hz for aliphatic and most aromatic protons) leads to insufficient destruction of ^{13}C bound protons for the determination of intermolecular NOEs. Several ways to improve basic X-filters have been described in the literature. Gemmecker et al. [23] used combinations of two X-filters optimized for ^{13}C–^{1}H one bond coupling constants of 125 and 140 Hz to suppress proton magnetization from both aliphatic and aromatic resonances. Separate suppression of aromatic signals can also be achieved by using selective 180° carbon pulses in the aromatic region during the evolution delay to shorten the time for creating antiphase magnetization on aromatic protons [13]. A sequence of up to five X-filtering blocks, within single scans, with differing evolution delays, was described by Kogler et al. [22] which gave a rather high theoretical efficiency in the absence of relaxation losses. Later on, the introduction of spin-lock and homo-spoil pulses allowed increased suppression of transverse magnetization for virtually all X-filters described [21]. It is noteworthy that in none of these, sometimes rather long, X-filters relaxation effects have been taken care of in the setup process, which might render their filtering efficiency unfavorable when used on macromolecular systems. Maybe the most efficient method for the filtering of ^{13}C-bound protons to date employs specially designed adiabatic carbon inversion pulses in the middle of a $90°(^{1}H)$–τ–$180°(^{1}H,^{13}C)$–τ–$90°(^{1}H)$–PFG building block [9,11]. It makes use of the fact that one-bond heteronuclear ^{1}H–^{13}C scalar coupling constants show an approximately linear correlation to the carbon chemical shift according to

$$^{1}J_{HC} = (0.365 \pm 0.01\,\mathrm{Hz/ppm})\delta_C + 120.0 \pm 0.5\,\mathrm{Hz}, \quad (1)$$

for proteins. Frequency swept WURST pulses [24] were designed to invert carbon spins at different times and allowing the one-bond coupling to evolve as a function of the carbon chemical-shift. However, for ^{1}H–^{13}C spin pairs with coupling constants deviating from the linear equation Eq. (1) the performance decreases. Here we present an easily implemented method that does not rely on Eq. (1), but suppresses ^{13}C-bound proton magnetization for a specified range of scalar coupling constants. In designing the described X-filter transverse proton relaxation has been included, which assures its filtering efficiency even in applications on biological macromolecules.

It should also be mentioned, that another different approach to separate the magnetization of ^{12}C- from ^{13}C-bound protons has been described by Melacini [17], where an additional *J*-resolved dimension is introduced into a ^{13}C-edited NOESY–HSQC. The necessary resolution was achieved by constant-time evolution of the $^{1}J_{CH}$ coupling. However, the long measurement time necessary for such a 4D experiment, might limit its application.

2. Theory

The basic building block of the X-filter used in the 3D ^{13}C-filtered, ^{13}C-edited NOESY–HSQC is shown in Fig. 1. The first 90° proton x-pulse creates in-phase ^{1}H y-magnetization, which evolves during τ_{in} under the influence of the ^{1}H-X one-bond coupling, while chemical shift evolution is refocused by the 180° proton pulse in the middle of τ_{in}. To obtain more efficient inversion of carbon and nitrogen nuclei, composite 180° pulses have been used [25]. The subsequent 90° proton pulse from the $-x$ direction flips the magnetization of protons, which did not experience scalar coupling evolution (i.e., ^{12}C- and ^{14}N-bound protons) back along the *z*-direction. Antiphase proton magnetization still present is then transformed into zero- and double quantum magnetization by the 90° carbon pulse [26]. Thereafter, any magnetization left in the *x*,*y*-plane is destroyed by the pulsed field gradient labeled G_2 in Fig. 1. The G_1 gradients are used to select for magnetization inverted by the 180° proton pulse in the middle of τ_{in}. As described above, such a ^{13}C-filter would destroy magnetization of protons one-bond coupled to a carbon with a coupling constant of $J = 1/(4 \times \tau_{in})$, but give only partial suppression for other $^{1}J_{HC}$ values. To overcome this drawback, this filter is repeated several times with varying delays τ_{in}. Relatively fast transverse relaxation in proteins and other large biomolecules prohibits the use of a large number of individual X-filters during a single transient. Therefore, we limited the number of filter elements per transient to three, setting the first one to 91 Hz, corresponding to typical ^{1}H–^{15}N one-bond coupling constants [18] since destruction of both ^{13}C- and ^{15}N-bound proton magnetization in a double-labeled macromolecule is necessary for the application described here. If magnetization of protons bound to

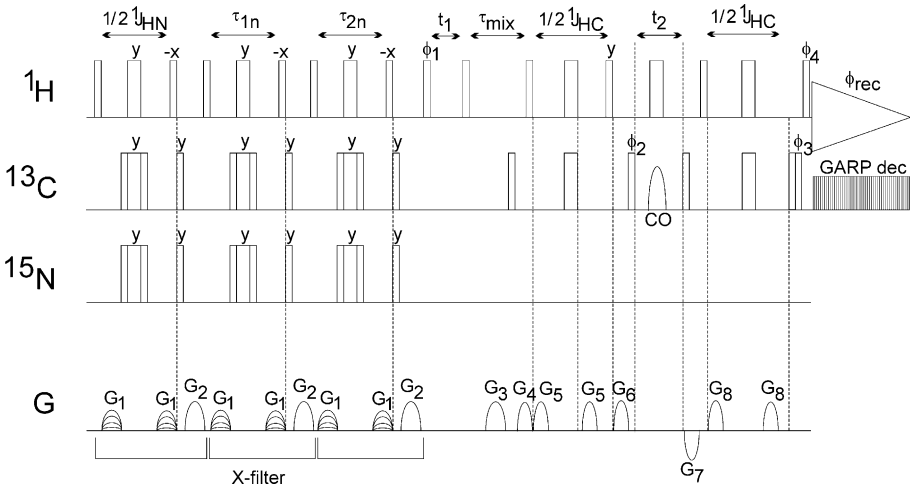

Fig. 1. Pulse sequence for the X-filter used in the 3D ^{13}C-filtered, ^{13}C-edited NOESY–HSQC. Thin and thick bars represent hard 90° and 180° pulses. The shaped pulse labeled CO is a soft 180° sinc pulse applied to the carbonyl region. All other pulses were applied in the middle of the typical spectral range of interest for proteins. For the applications described here we used the following carrier frequencies: ^{1}H, 4.76 ppm; ^{13}C, 39 ppm; ^{15}N, 119 ppm. Gradients labeled G_1, which select magnetization inverted by the 180° ^{1}H pulses during the X-filter, are varied between 3.7 and 8.3 G/cm and were applied during the whole $\tau_{in}/2$ period. G_2 destroys any magnetization left in the xy-plane and its power was set to 11.4 G/cm and the duration was 1 ms in all experiments. The other gradients had strengths of 3.2, 5.4, 4.8, 30, 19.3, and 8.6 G/cm and were applied for 3, 1, 1, 4, 3, and 1 ms for G_3, G_4, G_5, G_6, G_7, and G_8, respectively. All phases are x except when noted otherwise: $\phi_1 = x,x,x,x,-x,-x,-x,-x$, $\phi_2 = x,x,x,x,x,x,x,x,-x,-x,-x,-x,-x,-x,-x,-x$, $\phi_3 = x,x,x,x,-x,-x,-x,-x$, $\phi_4 = x,y,-x,-y$, $\phi_{rec} = x,-y,-x,y,-x,y,x,-y,-x,y,x,-y,x,-y,-x,y$. The scalar coupling evolution delays $1/2 \times {}^{1}J_{HN}$ and $1/2 \times {}^{1}J_{HC}$ were set to 5.5 and 3.6 ms corresponding to coupling constants of 91 and 140 Hz, respectively. τ_{mix} is the mixing time and τ_{in} are the evolution delays, which were optimized numerically (see text).

^{15}N is not suppressed, intramolecular ^{15}NH–^{13}CH NOEs will also be detected. To further increase the efficiency of the filtering scheme, the delays τ_{in} were not only varied within each transient but repeated with different values after a complete round of phase cycling. Completing the phase cycle before changing the τ_{in} values is necessary to avoid subtraction artifacts. So, for each t_1-increment n complete phase-cycling blocks were added.

The amount of magnetization on protons bound to ^{13}C, which is not destroyed by an individual filter block, is equal to $\cos(\pi J_{in})$ with J being the specific $^{1}J_{HC}$ scalar coupling constant of a ^{13}C–^{1}H fragment. Repeating this building block twice leads to an amount of residual magnetization for a specific one-bond carbon–proton coupling constant J, according to

$$I = I_0 \times \cos\left(\frac{\pi J}{2J_{HN}}\right) \times \prod_{i}^{2} \cos(\pi J \tau_{in}), \qquad (2)$$

where I is the amount of magnetization left from the starting magnetization I_0 after consecutive applications of the building block with varying delays τ_{in}. The magnetization left after adding k different sets of evolution delays τ_{in} after complete phase cycling rounds can be described by

$$I = I_0 \times \sum_{n}^{k} \left[\cos\left(\frac{\pi J}{2J_{HN}}\right) \times \prod_{i}^{2} \cos(\pi J \tau_{in}) \right]. \qquad (3)$$

The additional subscript n in the evolution delay τ_{in} accounts for the variation of the scalar coupling evolution delay in the X-filter building blocks after complete phase cycling rounds. Recently, we have described a somehow similar procedure for the selective excitation through destruction of off-resonance magnetization [27]. Thereby, a 90°x–τ_a–90°–x sequence is repeated several times with random variation of the interpulse delay τ_a, giving excitation in a narrow region on-resonance only. Randomization of the evolution delay is quite efficient for suppressing off-resonance magnetization since even small variations in the interpulse delay lead to vastly differing chemical shift evolutions. For scalar coupling constants a similar variation over several rotations of the magnetization vectors would last rather long due to the comparatively small size of coupling constants and hence cannot be applied to macromolecules. Therefore, the evolution delays τ_{in} have to be optimized in another way to achieve filtering for a large range of coupling constants. We found that simulated annealing [28,29] is perfectly suited for this purpose. As explained above, a series of three filter elements per transient, whereby the first evolution delay was set to eliminate $^{1}J_{HN}$ couplings, was chosen to keep relaxation losses to a minimum. Henceforth, the index of filter elements within a single transient (i), is the actual number of filter elements – 1, since the first scalar coupling evolution delay is kept constant. The number of variations between transients was set to 4 for all numerical optimizations, which gives sufficient filtering and keeps the necessary number of

transients for a full cycle reasonable. To obtain optimum suppression of ^{13}C-bound proton magnetization for $^1J_{HC}$ values between J_1 and J_2, by including transverse proton relaxation (T_2), a global minimum must be found for the following equation:

$$I = I_0 \times \int_{J_1}^{J_2} \left\{ \sum_n^4 \left[\cos\left(\frac{\pi J}{2J_{HN}}\right) \times e^{\frac{-1}{2J_{HN}T_2}} \times \prod_i^2 \cos(\pi J \tau_{in}) \times e^{\frac{-\tau_{in}}{T_2}} \right] \right\}^2 dJ. \quad (4)$$

The function inside the integral has to be squared to minimize any deviations (positive or negative) from zero. In Eq. (4) there are four parameters (two different τ_{in} values per transient with four alternations after complete rounds of phase cycling) that need to be varied during the simulated annealing process. Optimized sets of evolution delays have been calculated for various different transverse relaxation times. In addition a set of τ_{in} minimized for a wide range of T_2 values has been obtained by double integration of Eq. (4) over both J and T_2. Details about the simulated annealing procedure are described in the Section 5. Including T_2 relaxation times of protons bound to ^{13}C during the simulated annealing process is necessary to achieve high levels of suppression of heteronuclear bound proton magnetization. On the other hand, the length of the whole filtering sequence might lead to significant signal loss of protons bound to ^{12}C in large biomolecules. To reduce this loss of magnetization to a more reasonable extent, while keeping a decent filtering capacity, we introduced an additional $1 - e^{-\tau_{in}/T_2(^{12}C)}$ term into Eq. (4), when calculating τ_{in} values for very fast relaxing systems.

$$I = I_0 \times \left(f \times \sum_n^4 1 - e^{\frac{-1}{2J_{HN}T_2(^{12}C)} + \sum_i^2 \frac{-\tau_{in}}{T_2(^{12}C)}} \right) \times \int_{J_1}^{J_2} \left\{ \sum_n^4 \left[\cos\left(\frac{\pi J}{2J_{HN}}\right) \times e^{\frac{-1}{2J_{HN}T_2}} \times \prod_i^2 \cos(\pi J \tau_{in}) \times e^{\frac{-\tau_{in}}{T_2}} \right] \right\}^2 dJ. \quad (5)$$

$T_2(^{12}C)$ is used to describe the relaxation time of ^{12}C-bound protons, which is roughly twice as long as T_2 for ^{13}C-bound protons [18]. The constant f has been introduced in Eq. (5) in order to regulate the influence of the additional relaxation loss minimizing term. Hence, if filtering efficiency is the main criterion f should be small, and when magnetization losses during the long filter period need to be kept low f must be increased. We found that for f a value of approximately 0.1 enhances the signal intensity by up to 50% for fast relaxing protons, while still keeping the calculated residual magnetization of ^{12}C-bound protons below 1% in the $^1J_{CH}$ range between 120 and 160 Hz, which is typically the percentage of isotopic labeling achievable by standard techniques.

3. Results and discussion

Sets of evolution delays τ_{in} as obtained through simulated annealing optimization of Eqs. (4) and (5) for various specific transverse relaxation times are given in Table 1. Hereby, for T_2 down to 30 ms, corresponding to $T_2(^{12}C)$ of approx. 60 ms, Eq. (4) and for $T_2 = 20$ and 10 ms Eq. (5) with f set to 0.1 was used, respectively. The calculated residual magnetization is shown in Fig. 2a as a function of $^1J_{HC}$, where the theoretical residual magnetization of ^{13}C-bound protons is shown for T_2 values of 1000, 100, 50, 30, 20, and 10 ms as indicated. As can be seen, the calculated suppression of one-bond ^{13}C-coupled proton is always better than 1:1000 if the transverse relaxation time is known, a τ_{in} set optimized for this T_2 value is used and no emphasis is placed on reducing $T_2(^{12}C)$ losses. A significant decrease in filtering efficiency is observed if the filter optimization includes optimization of $T_2(^{12}C)$ signal loss as seen in Fig. 2a.

In cases where the transverse proton relaxation time T_2 is not known a set of τ_{in} values optimized not only for a range of $^1J_{HC}$ values (120–160 Hz) but also a whole range of T_2 times (20–200 ms) can be used. The residual magnetization for these τ_{in} values as a function of $^1J_{HC}$

Table 1
Sets of τ_{in} values (in μs) optimized for various transverse relaxation times T_2 and a $^1J_{HC}$ range between 120 and 160 Hz

	τ_{in}[μs]													
	$T_2 = 1000$ ms		$T_2 = 100$ ms		$T_2 = 50$ ms		$T_2 = 30$ ms		$T_2 = 20$–200 ms		$T_2 = 20$ ms		$T_2 = 10$ ms	
	$i = 1$	$i = 2$	$i = 1$	$i = 2$	$i = 1$	$i = 2$	$i = 1$	$i = 2$	$i = 1$	$i = 2$	$i = 1$	$i = 2$	$i = 1$	$i = 2$
$n = 1$	3804	2285	2877	2224	2045	2972	4783	5439	3347	5046	2083	1559	1446	1825
$n = 2$	3485	3440	5268	3435	2685	4067	2581	4251	3522	2976	1852	7888	2959	4115
$n = 3$	3057	3551	3960	2161	3316	10,261	7504	2076	4126	3420	2276	1707	2407	4030
$n = 4$	11,091	2827	10,318	3150	3338	5327	9526	6569	4151	10,022	2284	6974	7963	1143

i describes the position within the X-filter, whereas n is the count of complete phase cycles. So, for each transient the duration of the second and third X-filter is set to $1/2J$ values corresponding to the τ_{in} given for $i = 1$ and 2, respectively. For each single t_1-increment four complete rounds of phase cycling are repeated with the τ_{in} values given for $n = 1$–4. For the τ_{in} values corresponding to 10 and 20 ms relaxation losses were minimized using Eq. (5), whereas Eq. (4) was used for the other parameter sets.

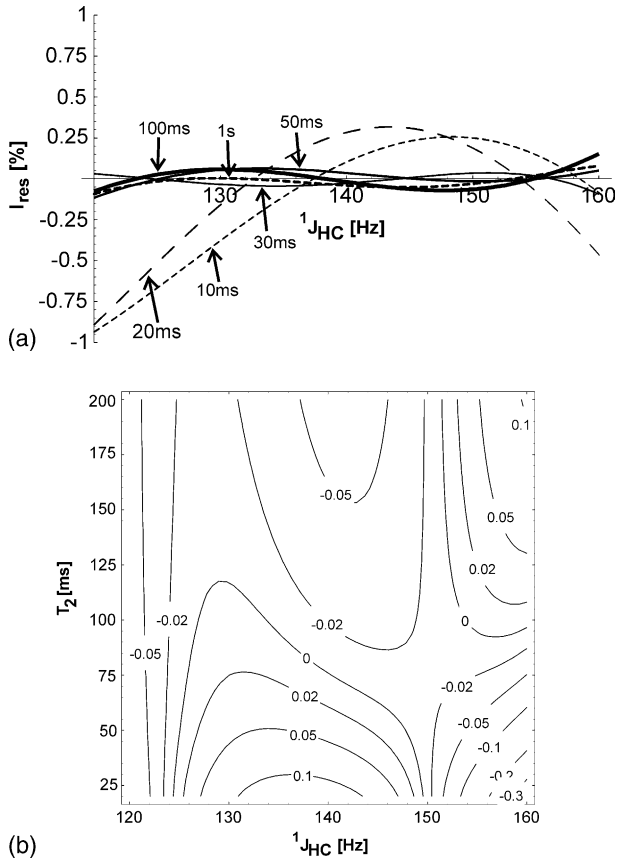

Fig. 2. The theoretical residual magnetization after the application of the presented X-filter optimized for T_2 values of 1 s, 100, 50, 30, 20, and 10 ms is shown in (a) as the percentage of its equilibrium value. For the curves corresponding to 10 and 20 ms relaxation losses were minimized using Eq. (5), whereas Eq. (4) was used for the other parameter sets. A set of τ_{in} values optimized for the range of transverse relaxation times between 20 and 200 ms (Table 1) was used for the calculation of residual magnetization (in % of equilibrium magnetization) as a function of $^1J_{HC}$ and T_2 in (b).

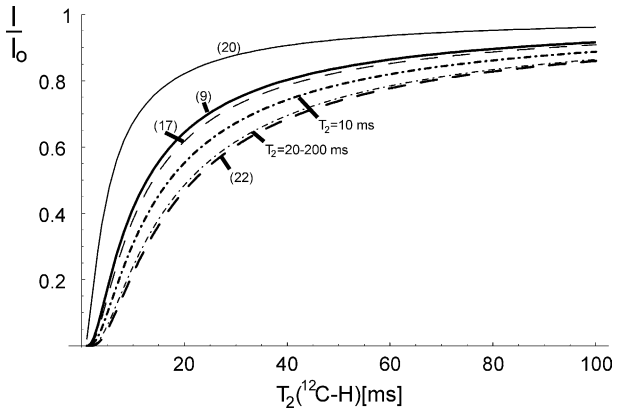

Fig. 3. Calculated intensity losses for various X-filters shown as a function of ^{12}C-bound proton transverse relaxation times. Shown are theoretical curves for: the most basic filtering scheme consisting of just one $90°(^1H)$–$\tau(1/4^1J_{HC})$–$180°(^1H, ^{13}C)$–$\tau(1/4^1J_{HC})$–$90°(^1H, ^{13}C)$ building block [20] (thin line), the method of Kay and co-workers [9], employing adiabatic pulses (thick line), the *J*-resolved 4D-NOESY–HSQC [17] (thin dashed line), the presented X-filter using τ_{in} values for $T_2 = 10$ ms (thick dot-dashed line), the presented X-filter using τ_{in} values for $T_2 = 20$–200 ms (thin dot-dashed line) and the X-filter consisting of five filter elements by Kogler et al. [22] (thick dashed line). The numbers shown denote the corresponding literature reference.

and T_2 relaxation times is shown in Fig. 2b. For the most part it is less than 0.1% of the equilibrium magnetization and it never exceeds 0.5%. Such high levels of suppression of magnetization of ^{13}C-bound protons can be used in the demanding application of determining intermolecular NOEs in a mixture of a labeled and an unlabeled compound. It should be noted, that suppression levels on the order 1:1000 are definitely higher than the enrichment available using standard labeling strategies. So, even if all magnetization of ^{13}C-bound protons could be destroyed, there would still be ^{1}H magnetization left in the labeled protein resulting from residual ^{12}C nuclei in the range of 1% or more. Therefore, to avoid the need for calculating new sets of evolution delays for every new system studied, it suffices to use the values optimized for the range of T_2 times for most macromolecular systems. As mentioned above, proton relaxation during the filter period leads to signal loss, which might become significant in very fast relaxing systems. To estimate this reduction in signal intensity a comparison of calculated relative intensities is shown in Fig. 3 for a number of different heteronuclear filtering schemes as a function of $T_2(^{12}C)$. The additional relaxation term of Eq. (5) was used for the calculation of these signal losses for the X-filter described herein, and single exponential transverse proton relaxation was assumed for the other heteronuclear filters shown in Fig. 3. The highest signal/noise ratio, (but worst filtering efficiency) is obtained using the most basic filtering scheme consisting of just one $90°(^1H)$–$\tau(1/4^1J_{HC})$–$180°(^1H, ^{13}C)$–$\tau(1/4^1J_{HC})$–$90°(^1H, ^{13}C)$ building block [20] (Fig. 3, thin line). The other curves shown in Fig. 3 correspond to the method of Kay and co-workers [9], employing adiabatic pulses (thick line), the *J*-resolved 4D–NOESY–HSQC [17] (thin dashed line), the presented X-filter using τ_{in} values for $T_2 = 10$ ms (thick dot-dashed line), the presented X-filter using τ_{in} values for $T_2 = 20$–200 ms (thin dot-dashed line) and the X-filter consisting of five filter elements by Kogler et al. [22] (thick dashed line). As can be seen, for very short relaxation times, the method proposed herein leads to rather significant reductions in signal/noise for very fast relaxing systems. However, the main focus has been put on achieving a high filtering efficiency over a broad range of heteronuclear one-bond coupling constants.

It should be pointed out that the efficiency of the presented filter results from the summation over three independent evolution delays and that "optimizing" the first filter element by shifting the 180° ^{13}C pulse to an effective $^1J_{HC}$ typical for H–C fragments does not improve the overall filtering capacity. For the same reason

shifting the 180° ^{15}N pulses in the second and third filter elements does not lead to any improvements. In fact, such shifting of pulses had detrimental effects on experimental spectra (data not shown), presumably due to changes in timing as a result of additional pre- and post-pulse delays and their asymmetric distribution within each filter element.

For the present study, the search for intermonomer NOEs in the homodimeric 18 kDa bacterial antidote ParD [30,31] was carried out with the pulse-sequence of Fig. 1. ParD is an 83-amino-acid protein from the post-segregational killing module of the broad-host-range plasmid RP4/RK2, which exercises two different control functions, an autoregulatory function by binding to its own promoter *PparDE* and a plasmid stabilizing function by inhibiting ParE toxicity in cells which express ParD and ParE. Since the protein functions as a dimer, the distinction of intermolecular from intramolecular NOEs has been essential for the determination of the 3D solution structure of this protein (to be described elsewhere). The efficiency of the X-filter in the 3D ^{13}C-filtered-^{13}C-edited NOESY–HSQC can be evaluated on the first increment by setting the NOE mixing time to zero. A comparison of such 1D spectra for various types of X-filters is shown in Fig. 4, where the excellent suppression of ^{13}C-bound proton magnetization by using the presented X-filter becomes obvious. Comparing the first increment of the same experiment with a mixing time of 150 ms (Fig. 4d) allows an estimation of the intensities of residual signals compared to true NOE signals. The residual magnetization in Fig. 4c leads to very small NOEs, which should be clearly separable from the true intermolecular NOEs, especially when their signal intensities are compared to the ones in a regular 3D NOESY–HSQC of fully labeled protein. A comparison of various 2D proton–proton planes at carbon chemical shifts of 18 ppm (Figs. 5a and b) and 59 ppm (Figs. 5c and d) in a regular (Figs. 5a and c) and a ^{13}C-filtered, ^{13}C-edited 3D NOESY–HSQC (Figs. 5b and d) is shown in Fig. 5, where assigned peaks are labeled by the residue number. Intermolecular NOEs are indicated by the residue number + 100 in the indirect dimension. The experiment used for the spectra in Fig. 5b and d not only eliminated intraresidue NOEs but also shows highly reduced or even missing signals on the diagonal, allowing easier interpretation of this spectrum. The intermolecular NOEs of ParD identified with the help of the pulse sequence in Fig. 1 are in very good agreement with a structural model obtained by gene-threading based on sequence homologies with the other DNA-binding, ribbon-helix–helix protein CopG [32].

Intermolecular NOEs are not only used to determine dimerization or oligomerization interfaces, but can also be used to find protein–ligand interaction areas for relatively tight complexes [10,33–35]. As a fast way of screening sequentially assigned proteins for their interaction interface with an unlabeled ligand, Eichmüller et al. [34] have recently proposed to use NOE difference spectroscopy with a 2D ^{13}C–^{1}H–HSQC as the readout

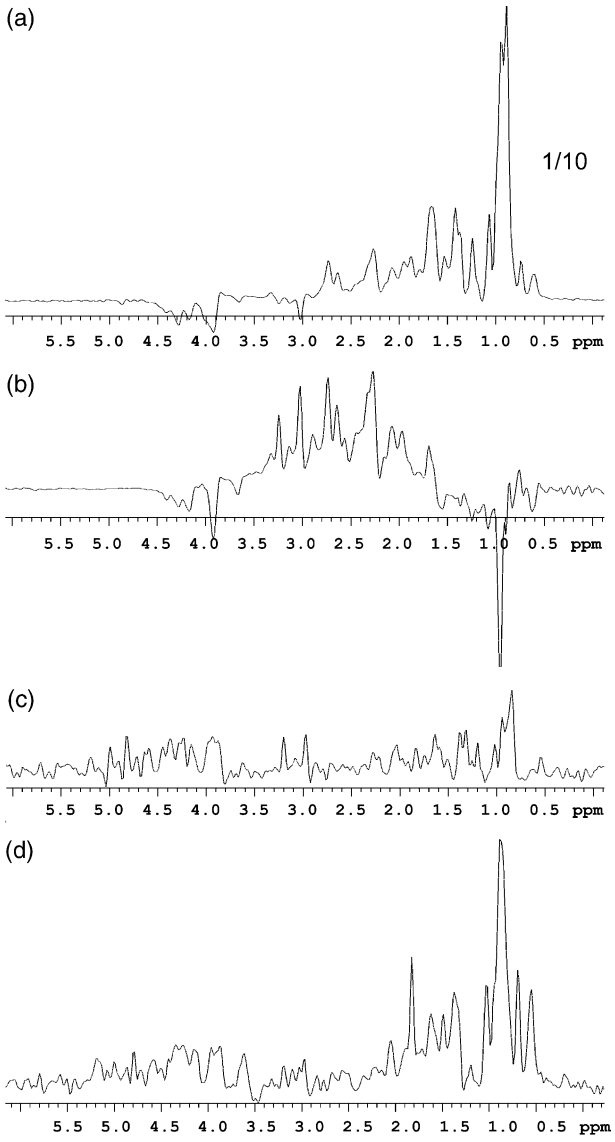

Fig. 4. Improved filtering using the presented purging scheme shown in the first increments of 3D ^{13}C-filtered, ^{13}C-edited NOESY–HSQC experiments on the 18 kDa homodimeric protein ParD consisting of a 0.7 mM 1:1 mixture of ^{13}C, ^{15}N double-labeled and unlabeled protein. (a) Using only the basic 90°(^{1}H)–1/4$^{1}J_{HC}$–180°(^{1}H, ^{13}C)–1/4$^{1}J_{HC}$–90° (^{13}C) X-filter. (b) Using specially designed adiabatic inversion pulses as described by Zwahlen et al. [9] and the spectrum in (c) was obtained employing the pulse-sequence of Fig. 1. For all these spectra the mixing time was set to 0 ms, whereas a mixing time of 150 ms was used for the first increment shown in (d), which was obtained with the same sequence as (c). For all spectra 64 transients of 2048 complex data points were accumulated and multiplied with a 60° phase shifted squared sine bell window function prior to Fourier transformation. The spectra are shown with the same vertical scale except (a) which was reduced by a factor of 10 because of huge amounts of unsuppressed magnetization compared to the other techniques.

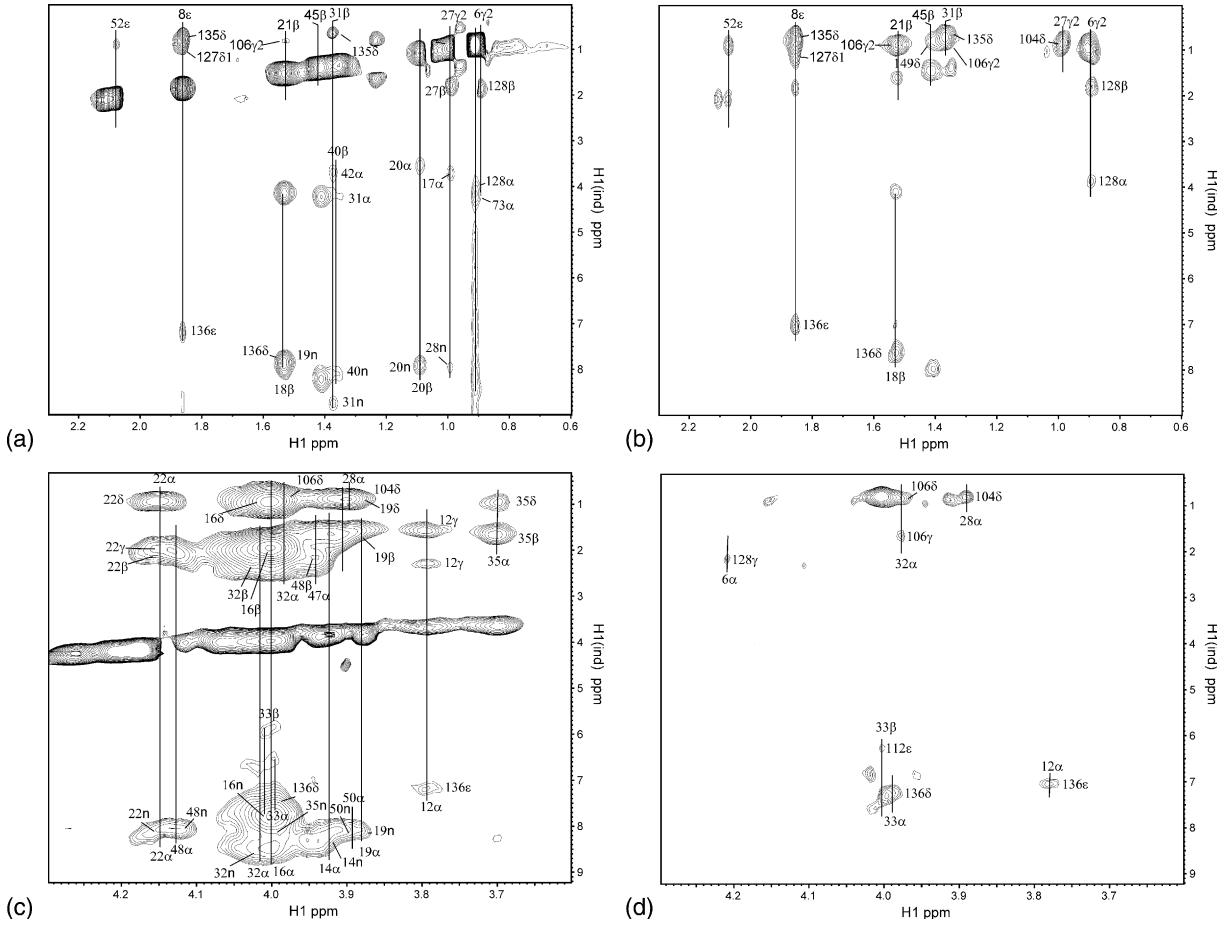

Fig. 5. 2D planes taken from (a, c) the 3D NOESY–HSQC and (b, d) the ^{13}C-filtered, ^{13}C-edited NOESY–HSQC on a 0.7 mM sample of a 1:1 mixture of ^{13}C, ^{15}N-labeled and unlabeled ParD. The planes are taken at ^{13}C frequencies of (a, b) 18.0 ppm and (c, d) 59.0 ppm. The protons belonging to the direct ^{1}H dimensions are labeled on top or below vertical lines, whereas peak annotations for the indirect proton dimensions are marked to the left or right of the corresponding peaks. Intermolecular NOEs are marked with the residue number + 100 in the indirect dimension. For both spectra data matrices of 2048 × 36 × 40 (^{1}H × ^{1}H × ^{13}C) complex data points were acquired and zero filled to 2048 × 256 × 256 points. In all dimensions 60° phase shifted squared sine bell window functions were applied prior to Fourier transformation. Sixty-four transients per increment were acquired for the ^{13}C-filtered, ^{13}C-edited NOESY–HSQC, and 16 for the regular NOESY–HSQC. Carrier positions were set to 4.76, 39, and 119 ppm for ^{1}H, ^{13}C, and ^{15}N, respectively, and sweep widths of 9000, 9000, and 18,000 Hz (^{1}H direct, ^{1}H indirect, and ^{13}C) were used.

spectrum. Thereby, the magnetization of protons from the unlabeled ligand is selectively inverted by a $90°(^{1}H)$–$1/4^{1}J_{HC}$–$180°(^{1}H, ^{13}C)$–$1/4^{1}J_{HC}$–$90°(^{1}H)$ sequence and after an isotropic mixing period, a ^{13}C-edited 2D HSQC acquired. The intensities of peaks in this experiment are compared to the same experiment where the carbon transmitter is offset during the X-filter. Differences in signal intensities point towards spin pairs correlated by cross relaxation (NOEs). To overcome the relatively poor destruction of magnetization of protons one-bond coupled to carbons, another set of 2D HSQCs with 0 ms isotropic mixing time has to be acquired.

The pulse-sequence of Fig. 1 carried out without incrementation of t_1 gives a 2D ^{13}C-edited HSQC showing only those protons that have an NOE to a proton bound to C-12 Fig. 6b. For comparison, a regular ^{13}C-HSQC of the same protein is shown in Fig. 6a. Since, artifacts present after 0 ms mixing time are not moved to a diagonal like in the 3D ^{13}C-filtered, ^{13}C-edited NOESY–HSQC (see above) they must be eliminated completely. This can be done by subtracting a similar 2D version with 0 ms mixing time. Residues belonging to peaks present in this 2D ^{13}C-filtered, ^{13}C-edited NOESY–HSQC of ParD correlate very well with residues found in the dimerization interface of this protein (Fig. 6c).

4. Conclusions

A simple and efficient X-filter consisting of an array of $90°(^{1}H)$–$1/4^{1}J_{HX}$–$180°(^{1}H, X)$–$1/4^{1}J_{HX}$–$90°(^{1}H, X)$–PFG building blocks has been presented. It employs numerically optimized variation of evolution delays, and pulsed field gradients for the suppression of ^{13}C-bound proton magnetization. By including

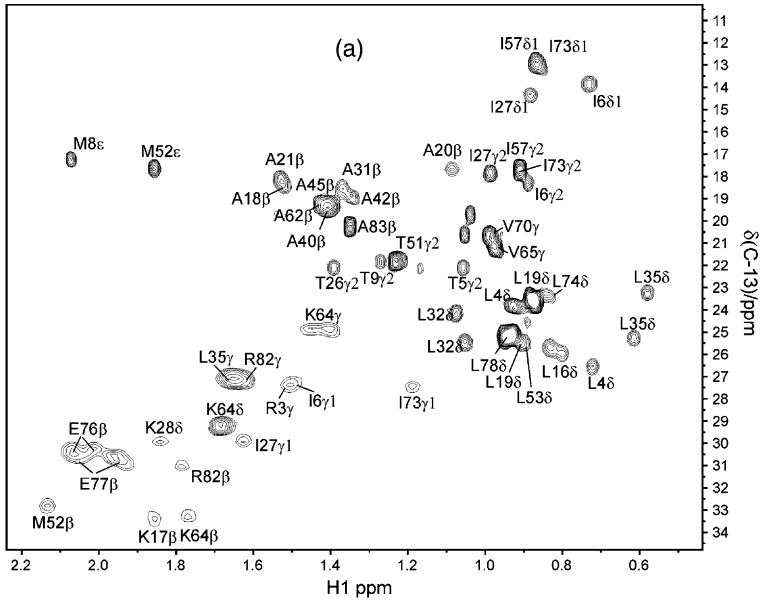

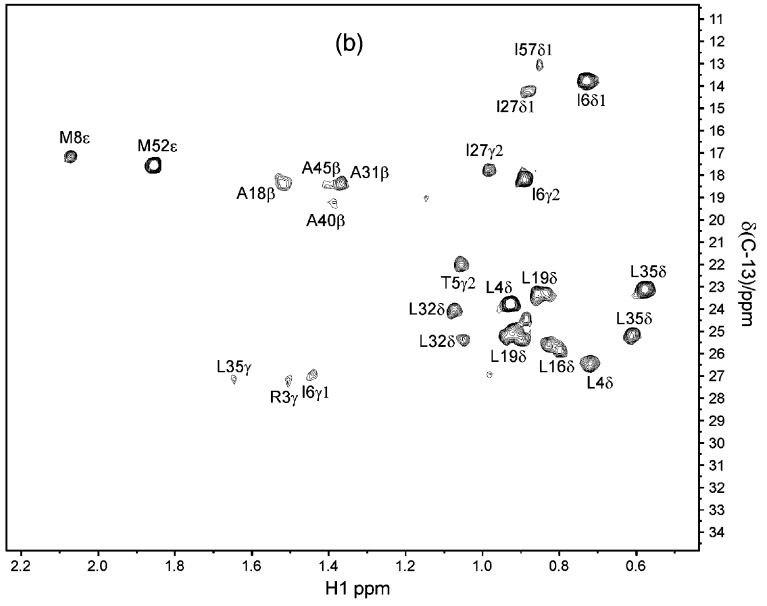

(c)

```
1           11          21          31          41
MSRLTIDMTD  QQHQSLKALA  ALQGKTIKQY  ALERLFPGDA  DADQAWQELK

51          61          71          81
TMLGNRINDG  LAGKVSTKSV  GETLDEELSG  DRA
```

Fig. 6. Upfield region of (a) a regular 2D ^{13}C–^{1}H HSQC and (b) a 2D version of the experiment shown in Fig. 1 without incrementation of t_1 acquired on 0.7 mM samples containing a 1:1 mixture of double-labeled and unlabeled ParD. For (b) a data set with 0 ms mixing time was subtracted from one with 150 ms mixing time to remove any artifacts still present in Fig. 3d. Sixty-four transients were accumulated for each of the 256 increments in both spectra and after zero filling to data matrices of 2k × 1k complex points in both dimensions, 60° phase shifted squared sine bell window functions were applied prior to Fourier transformation. The amino acid sequence of ParD is shown in (c) where residues found in the interaction interface are underlined and those found in the 2D ^{13}C-filtered, ^{13}C-edited NOESY–HSQC are in boldface letters.

transverse relaxation during the design of the presented X-filter, the high efficiency of the filter is maintained even in fast relaxing systems enabling the application to biological macromolecules. An easy set-up is combined with an efficiency high enough to allow for the observation of intermolecular NOEs through a 3D ^{13}C-filtered, ^{13}C-edited NOESY–HSQC as demonstrated on the 18 kDa homodimeric protein ParD. Fast screening of dimerization

or interaction interfaces can be achieved by recording a 2D version of the same experiment resulting in a 2D ^{13}C–^{1}H–HSQC showing only resonances that give rise to intermolecular NOEs.

5. Experimental

All calculations were carried out with Mathematica 4.0 [36] on a PC with AMD Athlon 1.3 GHz processor. The variables optimized during the simulated annealing process are the evolution delays $\tau_{in} = 1/2J_{in}$. The J_{in} values, were altered according to $J'_{in} = J_{in} + R_{in}\Delta_{in}$, with R_{in} being a random number between -1 and $+1$ and Δ_{in} the step size which was set to 1 Hz. The energy function used in the simulated annealing procedure is simply the integrated amount of squared residual magnetization described by Eqs. (4) or (5), where the integral was taken between 120 and 160 Hz. Each variable change corresponds to a jump on the energy surface, which is accepted if it leads to a lower energy. Uphill jumps are accepted if the probability $P_{up} = e^{\frac{\Delta E}{kT}}$ is less than a random number between 0 and 1. At the beginning of the simulated annealing process the product kT is set high enough to allow basically every change in parameters and therefore enable sufficient screening on the energy surface. For the present application, kT was decreased from 0.001 to 0.0 in 300 linear steps of size 3.3×10^{-6}. At each temperature the complete set of variables was changed 100 times. The whole simulated annealing procedure took about 90 min on the hardware described above.

All NMR experiments were carried out on a Varian Unity INOVA 600 MHz NMR spectrometer equipped with three rf-channels and z-axis gradients, using a 5 mm HCN triple resonance probe. The FIDs were multiplied with a 60° shifted squared sine bell window function in all dimensions prior to Fourier transformation. Other acquisition and processing parameters are given in the figure captions. All spectra were processed with NMRPipe [37]. The overall proton transverse relaxation time of ParD, as obtained through a 1D version of the CPMG sequence was around 42 ms and the τ_{in} set optimized for a T_2 of 30 ms was used for all experiments. The pulse-sequence and a parameter set for Varian INOVA spectrometers as well as the Mathematica script for the calculation of τ_{in} values can be obtained from the authors upon request.

^{13}C, ^{15}N-labeled ParD was expressed in minimal media with 1.5 g/L $(NH_4)_2SO_4$ as the sole nitrogen and 2 g/L ^{13}C-glucose as the sole carbon source in *Escherichia coli* BL21 as described [30,31]. A sample of 0.7 mM mixture of unlabeled and ^{13}C, ^{15}N-labeled ParD (i.e., 0.35 mM double-labeled protein) in H_2O/D_2O (90%/10%) in 20 mM phosphate buffer pH 6.0 was used for all experiments at 25 °C.

Acknowledgments

K.Z. thanks the Austrian Academy of Sciences for an APART fellowship (APART-692). Funding of this project has been provided by grants from the Austrian Science Foundation (P-14847 to K.Z., P-12559 to W.K. and P-13909 to H.S.).

References

[1] G.M. Clore, A.M. Gronenborn, New methods of structure refinement for macromolecular structure determination by NMR, Proc. Natl. Acad. Sci. USA 95 (1998) 5891–5898.
[2] G.M. Clore, A.M. Gronenborn, NMR structures of proteins and protein complexes beyond 20,000 M(r), Nat. Struct. Biol. 4 (Suppl) (1997) 849–853.
[3] K. Wüthrich, The second decade–into the third millenium, Nat. Struct. Biol. 5 (Suppl) (1998) 492–495.
[4] D. Neuhaus, M. Williamson, The nuclear Overhauser effect in structural and comformational analysis, VCH Publishers, New York, 1989.
[5] L.E. Kay, J.D. Forman-Kay, W.D. McCubbin, C.M. Kay, Solution structure of a polypeptide dimer comprising the fourth Ca(2+)-binding site of troponin C by nuclear magnetic resonance spectroscopy, Biochemistry 30 (1991) 4323–4333.
[6] J.N. Breg, J.H. van Opheusden, M.J. Burgering, R. Boelens, R. Kaptein, Structure of Arc repressor in solution: evidence for a family of β-sheet DNA-binding proteins, Nature 346 (1990) 586–589.
[7] M. Weiss, Distinguishing symmetry-related intramolecular nuclear Overhauser effects in a protein by asymmetric isotopic labeling, J. Magn. Reson. 86 (1990) 626–632.
[8] C.H. Arrowsmith, R. Pachter, R.B. Altman, S.B. Iyer, O. Jardetzky, Sequence-specific ^{1}H NMR assignments and secondary structure in solution of *Escherichia coli* trp repressor, Biochemistry 29 (1990) 6332–6341.
[9] C. Zwahlen, P. Legault, S.J.F. Vincent, J. Greenblatt, R. Konrat, L.E. Kay, Methods for the measurement of intermolecular noes by multinuclear NMR spectroscopy: application to a bacteriophage λ N-Peptide/*box*B RNA Complex, J. Am. Chem. Soc 119 (1997) 6711–6721.
[10] S.M. Pascal, A.U. Singer, G. Gish, T. Yamazaki, S.E. Shoelson, T. Pawson, L.E. Kay, J.D. Forman-Kay, Nuclear magnetic resonance structure of an SH2 domain of phospholipase C-γ 1 complexed with a high affinity binding peptide, Cell 77 (1994) 461–472.
[11] C. Eichmüller, W. Schüler, R. Konrat, B. Kräutler, Simultaneous measurement of intra- and intermolecular NOEs in differentially labeled protein–ligand complexes, J. Biomol. NMR 21 (2001) 107–116.
[12] P.J.M. Folkers, R.H.A. Folmer, R.N.H. Konings, C.W. Hilbers, Overcoming the ambiguity problem encountered in the analysis of nuclear Overhauser magnetic resonance spectra of symmetric dimer proteins, J. Am. Chem. Soc 115 (1993) 3798–3799.
[13] R.H.A. Folmer, C.W. Hilbers, R.N.H. Konings, K. Hallenga, A ^{13}C double-filtered NOESY with strongly reduced artefacts and improved sensitivity, J. Biomol. NMR 5 (1995) 427–432.
[14] M. Ikura, A. Bax, Isotope-filtered 2D NMR of a protein–peptide complex: Study of a skeletal muscle myosin light chain kinase fragment bound to calmodulin, J. Am. Chem. Soc 114 (1992) 2433–2440.
[15] A.P. Eijkelenboom, R.A. Lutzke, R. Boelens, R.H. Plasterk, R. Kaptein, K. Hard, The DNA-binding domain of HIV-1 integrase has an SH3-like fold, Nat. Struct. Biol. 2 (1995) 807–810.
[16] M.J. Burgering, R. Boelens, M. Caffrey, J.N. Breg, R. Kaptein, Observation of inter-subunit nuclear Overhauser effects in a

dimeric protein. Application to the Arc repressor, FEBS Lett. 330 (1993) 105–109.
[17] G. Melacini, Separation of intra- and intermolecular NOEs through simultaneous editing and J-compensated filtering: A 4D quadrature-free cinstant-time *J*-resolved approach, J. Am. Chem. Soc. 122 (2000) 9735–9738.
[18] J. Cavanagh, W.J. Fairbrother, A.G. Palmer, N.J. Skelton, Protein NMR Spectroscopy, Academic Press, San Diego, 1996.
[19] G. Otting, K. Wüthrich, Extended heteronuclear editing of 2D 1H NMR spectra of isotope-labeled proteins, using the X($\omega 1, \omega 2$) double half filter, J. Magn. Reson. 85 (1989) 586–594.
[20] G. Otting, H. Senn, G. Wagner, K. Wüthrich, Editing of 2D ^{1}H NMR spectra using X half filters. Combined use with residue-selective 15N labeling of proteins, J. Magn. Reson. 70 (1986) 500–505.
[21] G. Otting, K. Wüthrich, Efficient purging scheme for proton-detected heteronuclear two-dimensional NMR, J. Magn. Reson. 76 (1988) 569–574.
[22] H. Kogler, O.W. Sorensen, G. Bodenhausen, R.R. Ernst, Low-pass J filters. Suppression of neighbor peaks in heteronuclear relayed correlation spectra, J. Magn. Reson. 55 (1983) 157–163.
[23] G. Gemmecker, E.T. Olejniczak, S.W. Fesik, An improved method for seletively observing protons attached to ^{12}C in the presence of ^{1}H–^{13}C spin pairs, J. Magn. Reson. 96 (1992) 199–204.
[24] E. Kupce, R. Freeman, Adiabatic pulses for wide-band inversion and broad-band pulse, J. Magn. Reson. A 115 (1995) 273–276.
[25] M.H. Levitt, R. Freeman, NMR population inversion using a composite pulse, J. Magn. Reson. 33 (1979) 473.
[26] R.R. Ernst, G. Bodenhausen, A. Wokaun, Principles of Nuclear Magnetic Resonance in One and Two Dimensions, Clarendon Press, Oxford, 1994.
[27] K. Zangger, M. Oberer, H. Sterk, Pure-phase selective excitation in fast-relaxing systems, J. Magn. Reson. 152 (2001) 48–56.
[28] W.H. Press, S.A. Teukolsky, W.T. Vetterling, B.P. Flannery, in: Simulated Annealing Methods, Cambridge University Press, Cambridge, UK, 1992, pp. 436–448.
[29] H. Geen, R. Freeman, Band-selective radiofrequency pulses, J. Magn. Reson. 93 (1991) 93–141.
[30] M. Oberer, H. Lindner, O. Glatter, C. Kratky, W. Keller, Thermodynamic properties and DNA binding of the ParD protein from the broad host-range plasmid RK2/RP4 killing system, Biol. Chem. 380 (1999) 1413–1420.
[31] M. Oberer, K. Zangger, S. Prytulla, W. Keller, The anti-toxin ParD of plasmid RK2 consists of two structurally distinct moieties and belongs to the ribbon-helix–helix family of DNA-binding proteins, Biochem. J. 361 (2002) 41–47.
[32] F.X. Gomis-Ruth, M. Sola, P. Acebo, A. Parraga, A. Guasch, R. Eritja, A. Gonzalez, M. Espinosa, G. del Solar, M. Coll, The structure of plasmid-encoded transcriptional repressor CopG unliganded and bound to its operator, EMBO J. 17 (1998) 7404–7415.
[33] S.W. Fesik, J.R. Luly, J.W. Erickson, C. Abad-Zapatero, Isotope-edited proton NMR study on the structure of a pepsin/inhibitor complex, Biochemistry 27 (1988) 8297–8301.
[34] C. Eichmüller, M. Tollinger, B. Kräutler, R. Konrat, Mapping the ligand binding site at protein side-chains in protein–ligand complexes through NOE difference spectroscopy, J. Biomol. NMR 20 (2001) 195–202.
[35] H. Takahashi, T. Nakanishi, K. Kami, Y. Arata, I. Shimada, A novel NMR method for determining the interfaces of large protein–protein complexes, Nat. Struct. Biol. 7 (2000) 220–223.
[36] S. Wolfram, Mathematica, fourth ed., Wolfram Research Inc., Champaign, IL, 1999.
[37] F. Delaglio, S. Grzesiek, G.W. Vuister, G. Zhu, J. Pfeifer, A. Bax, NMRPipe: a multidimensional spectral processing system based on UNIX pipes, J. Biomol. NMR 6 (1995) 277–293.